Finite-Size Networks from Cylindrical Polyelectrolyte Brushes and Porphyrins

Christian Ruthard,[†] Michael Maskos,[‡] Ute Kolb,[‡] and Franziska Gröhn*,[†]

Max Planck Institute for Polymer Research, Ackermannweg 10, D-55128 Mainz, Germany, and Institut für Physikalische Chemie, Universität Mainz, Welder-Weg 11, D-55099 Mainz, Germany

Received September 6, 2008; Revised Manuscript Received October 30, 2008

ABSTRACT: We report on the electrostatic self-assembly of negatively charged cylindrical polystyrenesulfonate (NaPSS) brushes and stiff organic counterions of different valency. In particular, the tetravalent cationic porphyrin *meso*-tetrakis(4-(trimethylammonium)phenyl)porphyrin (TAPP) yielded two new supramolecular architectures that are stable in aqueous solution. The porphyrin binds to the polyelectrolyte brush due to electrostatic and secondary $\pi-\pi$ interactions and can further interconnect the brushes to nanoscale networks. In salt solution individual porphyrin-decorated cylindrical brushes were obtained. Structures formed are characterized by UV−vis spectroscopy, atomic force microscopy (AFM), cryo-transmission electron microscopy (cryo-TEM), small-angle neutron scattering (SANS), and dynamic light scattering (DLS). In order to study porphyrin aggregates by DLS, an IR laser setup ($\lambda = 831.5$ nm) was used. The new morphologies have potential as functional structures in molecular electronics and pharmaceutics.

Introduction

A variety of structures and functions in natural systems is realized by supramolecular systems, prominent examples being lipid bilayers, DNA−protein complexes, or cartilage. Because of their potential for functionality and responsiveness, the synthesis of supramolecular structures from the association of smaller building units has become an active area of research.[1] Bases for self-organization processes have been amphiphilicity,[2−6] hydrogen bonding,[7−10] metal coordination,[11] and ionic interaction. Ionic interaction leads to very well-defined and structured solid materials.[12−17] Studies on aggregates in solution predominantly cover the association of two oppositely charged polyelectrolytes[18,19] and polyelectrolytes with multivalent counterions.[20−26] Recently, we could show that a larger structural control can be realized if ionic components with a certain geometry are applied and secondary interactions between counterions in addition direct the structure formation.[27−29] For example, multivalent organic counterions are able to connect polyelectrolyte dendrimers into defined assemblies of different shape.[27−29] It is thus promising to extend the concept of electrostatic self-assembly toward nanoscale structures with different architectures and functionalities.

Cylindrical polyelectrolyte brushes represent a promising type of polyelectrolyte architecture: polymeric side chains connected to a polymer backbone force this backbone to adopt a more elongated conformation than in an usual polymer coil, resulting in semiflexible cylindrical molecules.[30−40] Depending on side chain length and total molecular mass, diameter and length can be varied. Typical values for brush lengths are 100−200 nm and for diameters 4−12 nm.[41] We here use samples that are prepared by the polymerization of macromonomers, resulting in narrowly distributed side chain length and thus diameter but also in a quite broad length distribution. Recently, it was shown that precipitated complexes of polyelectrolyte brushes with oppositely charged surfactants can be dissolved in an organic solvent, yielding individual brushes associated with surfactant molecules with slightly larger diameter than the initial brushes.[42] It seems thus promising to investigate cylindrical polyelectrolyte brushes having restricted flexibility as building units in electrostatic self-assembly with organic counterions in analogy to the mentioned dendrimer systems.

Porphyrins are intensively studied molecules due to their special function in natural systems such as in photosynthesis and oxygen transport and their potential capability to fulfill certain functions in synthetic systems: interest ranges from photosynthetic model systems[43−46] over photoconductive materials[47] to catalytic activity[48] and medical applications as tumor-localizing and photosensitizing agents.[49−51] In particular, functionalities where porphyrin stacks occur may be influenced or improved by using a polyelectrolyte template. Porphyrin stacks formed at high concentration without a template are difficult to control in size, and in particular it is still a problem to deposit them on surfaces without changing the aggregate size and architecture. This, however, is required for many applications or fundamental studies. A polymeric template may provide larger stability and processability. More than combining the properties of the polymer and the functional counterion, self-organization of both components may yield novel assemblies with interesting properties. With this background investigating the combination of polyelectrolyte brushes with multivalent porphyrins as counterions is expected to build a valuable step in establishing electrostatic self-assembly as a route to supramolecular structures in aqueous solution.

The gelation of synthetic and natural macromolecules has attracted increasing interest in recent years because of the numerous applications offered by self-assembling networks, for example in tissue engineering, drug delivery, or food technology.[52−54] Such structures usually emerge due to the presence of specific noncovalent interactions such as hydrogen bonding, $\pi-\pi$ stacking, and hydrophobic or electrostatic interactions. Additionally, the capacity of network formation may depend on the rigidity of the aggregating polymers. While rigid-chain macromolecules can self-assemble into three-dimensional networks by end-to-end aggregation, flexible polymers tend to form collapsed structures.[55]

In this contribution we studied the formation of nanoscale aggregates from negatively charged cylindrical polystyrenesulfonate brushes (NaPSS) and stiff organic counterions of different valency, in particular tetravalent cationic porphyrins

* Corresponding author: Fax 49-6131-379100; e-mail groehn@mpip-mainz.mpg.de.
[†] Max Planck Institute for Polymer Research.
[‡] Universität Mainz.

10.1021/ma802038q CCC: $40.75
Published on Web 01/16/2009

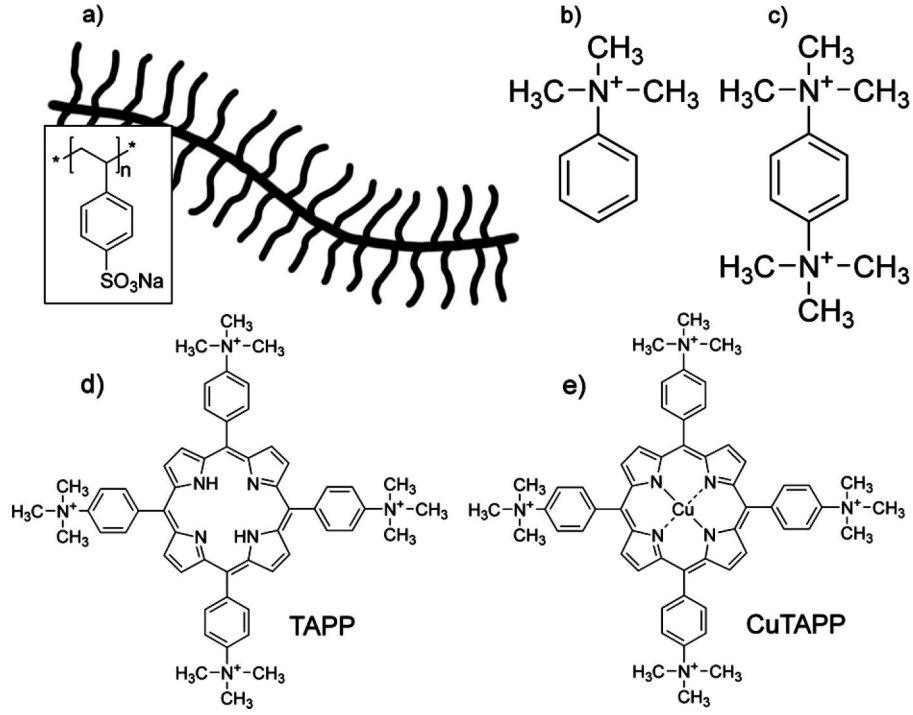

Figure 1. Ionic components used in this study: (a) architecture and molecular structure of negatively charged NaPSS polyelectrolyte brush; (b) monovalent counterion: trimethylphenylammonium chloride; (c) divalent counterion: *p*-phenylene bis(trimethylammonium tosylate); (d) tetravalent counterion: *meso*-tetrakis(4-(trimethylammonium)phenyl)porphyrin tetratosylate (TAPP); (e) tetravalent counterion: *meso*-tetrakis(4-(trimethylammonium)phenyl)porphyrin copper(II) tetrachloride (CuTAPP).

(Figure 1). Structures formed are characterized by UV−vis spectroscopy, atomic force microscopy (AFM), cryo-transmission electron microscopy (cryo-TEM), small-angle neutron scattering (SANS), and dynamic light scattering (DLS). To study porphyrin aggregates by DLS, a setup using an infrared laser has been set up.

Experimental Section

Counterions. *p*-Phenylene bis(trimethylammonium tosylate) was synthesized by stepwise methylation of *N*,*N*,*N*′,*N*′-tetramethyl-*p*-phenylenediamine with 6-fold excess of methyl *p*-toluenesulfonate at 60 °C for several hours first in nitromethane giving 60% monomethylated product and 40% dication as verified by ^{1}H NMR. In a second step the precipitate was redissolved in water (some ethanol was added to enhance solubility of methylating agent), and the reaction was carried out under otherwise identical conditions yielding a 96% divalent product. Twofold careful recrystallization from an ethanol/water mixture yielded 100% of the desired product.

meso-Tetrakis(4-(trimethylammonium)phenyl)porphyrin copper(II) tetrachloride (CuTAPP) was prepared from TAPP according to the literature.[56] Because of the binding of copper by the porphyrin ligand and the symmetry change from D_{2h} to D_{4h} the spectrum of CuTAPP exhibits only one main Q-band maximum at $\lambda = 539$ nm (not shown). This observation in combination with hypochromicity in comparison to TAPP is consistent with the literature[57] and thus proves that TAPP is completely transformed into CuTAPP.

All other chemicals including the porphyrin *meso*-tetrakis(4-(trimethylammonium)phenyl)porphyrin tetratosylate (TAPP) were bought from Aldrich and used as received. The structures were verified by ^{1}H NMR analysis. All TAPP and CuTAPP concentrations were calibrated from literature extinction coefficients using ε(TAPP) $= 4.16 \times 10^5$ M^{-1} cm^{-1} and ε(CuTAPP) $= 3.46 \times 10^5$ M^{-1} cm^{-1} at $\lambda = 412$ nm.[56]

Cylindrical Polystyrenesulfonate Brushes. A polystyrene macromonomer was synthesized by anionic polymerization of styrene and subsequent end-functionalization by *p*-vinylbenzyl chloride.[30,32,58,59] The macromonomer was characterized by MALDI-TOF giving $M_w = 4450$ g mol^{-1} with $M_w/M_n = 1.06$ from GPC analysis (defining the later side chain length of the polymer brush being 43). Free radical homopolymerization of this macromonomer yielded a polystyrene brush with $M_w = 2.13 \times 10^6$ g mol^{-1} and $M_w/M_n = 3.02$ (GPC). In order to obtain lower polydispersities, the polystyrene brush was fractionated by continuous polymer fractionation (CPF).[60] For this study a high molecular mass fraction with $M_w = 4.12 \times 10^6$ g mol^{-1} and $M_w/M_n = 1.51$ (weight-average degree of polymerization of the main chain $P_w = 900$) was chosen. The polystyrene brush was then sulfonated with sulfuric acid/acetic anhydride in 1,2-dichloroethane at 50 °C.[37,61] The precipitated product was isolated as the sodium salt by dissolution in aqueous NaOH (without prior drying) and subsequent removal of excess dichloroethane by evaporation and purification via ultrafiltration, resulting in a NaPSS brush with 100% sulfonation according to elemental analysis.[62]

Atomic Force Microscopy. We used a commercial MultiMode microscope operated in tapping mode with a Nanoscope IIIa controller and 12 × 12 μm E-scanner from Veeco Instruments, Santa Barbara, CA. An Olympus cantilever OMCL-AC160TS with a spring constant of 42 N/m and a nominal tip radius <10 nm was used after cleaning in argon plasma. Brush and porphyrin-brush samples were spin-coated for 120 s at 3000 rpm onto freshly cleaved mica and imaged in air (as they do not adsorb on a mica surface when just exposed to the solution). Porphyrin-brush samples in NaCl solution were prepared by adsorption to a mica surface: freshly cleaved mica was exposed to the solution for 5 min and then rinsed with water and blow-dried. This procedure was possible for this type of samples (for reasons see Results and Discussion) and in contrast to spin-coating removed excess salt. Images given are height images recorded in tapping mode with a height scale of maximum 20 nm.

Cryo-Transmission Electron Microscopy. Cryo-TEM images were recorded on a FEI Tecnai 12 at an acceleration voltage of 120 kV. Quantifoil copper grids with 2 μm holes were used for sample preparation. All samples were vitrified without any external staining from room temperature in liquid ethane using a FEI Vitrobot.

Light Scattering. Samples were filtered several times through Millipore cellulose acetate membrane filters with 0.22 μm pore size into Hellma quartz cuvettes with 2 cm internal diameter (for details see Results and Discussion). Measurements were carried out at 20 °C using an ALV 5000 correlator with 320 channels (ALV Langen, Germany) and a He−Ne laser (JDS Uniphase) with a wavelength of $\lambda = 632.8$ nm and 22 mW output power. For light absorbing samples containing porphyrins, an IR laser (Schäfter + Kirchhoff laser diode with single mode fiber and gauss profile) with a wavelength of $\lambda = 831.5$ nm and 80 mW output power was used. The scattered intensity was divided by a beam splitter (approximately 55:45), each portion of which was detected by a photomultiplier. The two signals were cross-correlated in order to eliminate nonrandom electronic noise. Measurements were performed in 10° steps at scattering angles of 30°−150° with the red and 50°−110° with the infrared laser.

Measurement and data analysis procedure were as established: the time autocorrelation function of the scattered intensity was measured (homodyne mode) and converted into the scattered electric field autocorrelation function via the Siegert relation. The electric field autocorrelation function was analyzed by second-order cumulant analysis:

$$\ln(g_1(\tau)) = -\Gamma\tau + \frac{\mu_2}{2}\tau^2 \quad (1)$$

The apparent diffusion coefficient was calculated from the inverse relaxation time and extrapolated to zero scattering vector square. The hydrodynamic radius was obtained via the Stokes−Einstein relation from the diffusion coefficient.

Small-Angle Neutron Scattering. Samples for SANS were prepared in D_2O with a polymer concentration of 1 g L^{-1} (4.8 mM) and transferred into optical quality quartz cells with 2 mm path length. SANS studies were performed at the FRM II, Munich, Germany, and at Institute Laue Langevin (ILL), Grenoble, France. Data shown result from the KWS 1 instrument of the Jülich Center for Neutron Science at FRM II using three configurations with the neutron wavelengths λ and sample−detector distances d of $\lambda = 0.45$ nm/$d = 1.6$ m, $\lambda = 0.45$ nm/$d = 7.6$ m, and $\lambda = 1.2$ nm/$d = 7.6$ m. A total scattering vector range of 0.034 $nm^{-1} < q < 3.0$ nm^{-1} was covered. Data were corrected for empty quartz cell scattering, electronic background, and detector uniformity and converted to an absolute scale using secondary standards. The data were further corrected by subtracting the contributions from solvent scattering and incoherent background. All measurements and data treatment have been performed according to common procedures. Experimental errors of $I(q)$ data are within 1% for $q < 0.6$ nm^{-1}, below 10% for $q < 1$ nm^{-1}, and increase up to 50% for highest q data.

Cross-section radii of gyration were determined from cross-section Guinier analysis:[63]

$$qI(q) = I_0 e^{-(q^2 R_{G,c}/2)} \quad (2)$$

Data were further analyzed according to the cylindrical geometry applying the Fourier transformation for cylindrical particles where the cross-section distribution function $P_c(r)$ is calculated via

$$qI(q) = 2\pi \int_{r=0}^{\infty} P_c(r) J_0(qr)\, dr \quad (3)$$

with $J_0(x)$ being the zero-order Bessel function, r the radial distance, and q the scattering vector magnitude.[64−67] The indirect transformation method is applied in order to minimize termination effects. We use the program ITP, indirect transformation for the calculation of $P(r)$, by Glatter which includes smoothing of the primary data by a weighted least-squares procedure (estimation of the optimum stabilization parameter based on a stability plot), desmearing, and transforming into real space simultaneously. The actual calculations dealing with the experimental scattering curves accounted for the measured beam profile and the wavelength distribution of the experimental setup.

UV−vis Spectroscopy. Spectra were recorded in Hellma optical quartz cuvettes (path length 1 cm) with Lambda 25 from Perkin-Elmer.

Results and Discussion

Figure 1 gives an overview of the building blocks investigated in this study. The divalent counterion *p*-phenylene bis(trimethylammonium tosylate) (c) was successfully synthesized as part of this study by stepwise methylation of *N*,*N*,*N*′,*N*′-tetramethyl-*p*-phenylenediamine using methyl *p*-toluenesulfonate. The structure was confirmed by NMR characterization. As compared to the diiodide, the synthesis of which is described in literature,[68] the ditosylate was preferred because of its higher water solubility.

Cylindrical brushes with side and main chain both consisting of polystyrene subunits were synthesized by the macromonomer approach[30,32,37,41,58,59] and subsequent sulfonation yielded the polystyrenesulfonate brush. The NaPSS brush of this study has a main chain average degree of polymerization $P_w = 900$, and each macromonomer consists of 43 styrenesulfonate subunits. The side chain length and thus the diameter of the brush are well-defined, whereas there is a distribution of the main chain length inherent to the macromonomer approach resulting in a polydispersity of $M_w/M_n = 1.5$. The degree of sulfonation was determined to be 100%; thus, the PSS brushes of this study are of the same type as the ones described in ref 37, but with a higher degree of sulfonation.

Characterization by static and dynamic light scattering yielded a molecular mass of $M_w = 7.81 \times 10^6$ g mol^{-1} and a weight-average contour length $L_w = 116$ nm of the cylindrical molecule in aqueous solution. At the concentration predominantly used in this study (c(NaPSS) = 240 μM) light scattering yielded $R_G = 50$ nm and $R_H = 36$ nm in salt-free aqueous solution and $R_G = 60$ nm and $R_H = 36$ nm in 10 mM NaCl solution, while no expressed concentration dependence was found in this concentration range. The ratio $\rho = R_G/R_H \approx 1.5$ is characteristic of rodlike molecules.

To prepare brush−counterion samples, aqueous solutions of polystyrenesulfonate brushes and counterions were mixed. The selected preparation procedure used throughout this study was adding a porphyrin stock solution to the brush solution under stirring. The reason for this and comparison of different preparation routes will be discussed in section E.

The PSS brush used is present as sodium salt. Addition of $c = 240$ μM trimethylphenylammonium chloride as monovalent counterion to a salt-free NaPSS solution of $c = 240$ μM leads to a sample with a hydrodynamic radius of $R_H = 38$ nm as measured by dynamic light scattering. This is close to the result obtained for pure brush. Thus, no interconnection of polyelectrolyte brushes was found. Combining the polyelectrolyte brush with the divalent counterion *p*-phenylene bis(trimethylammonium tosylate) likewise does not result in larger structural changes. Here again $R_H = 38$ nm at charge stoichiometry of counterion to brush was measured, and even in excess of divalent counterion no expressed size changes were found. Thus, more than two charges per counterion are necessary to interconnect brushes at the given concentration.

A. Observations and UV−vis Spectroscopy with Brush−Porphyrin Aggregates. The tetravalent counterion TAPP causes a very different behavior: changes are already visible by eye, as shown in Figure 2. While TAPP in aqueous solution shows a violet color (right), combination with the colorless brush solution (left) results in a light-brown solution (middle). Such spectral changes induced by $\pi-\pi$ interactions are well-known for porphyrins but usually observed at higher concentrations

Figure 2. Photograph demonstrating color shifts in water: left: NaPSS brush (c(NaPSS) = 240 μM); center: NaPSS brush with TAPP (c(NaPSS) = 240 μM, c(TAPP) = 30 μM, l = 0.5); right: TAPP (c(TAPP) = 30 μM).

only. Here we used a porphyrin concentration at which it usually is present in an unaggregated state (violet solution). Upon addition of PSS brush, the porphyrin electrostatically binds to the oppositely charged polyelectrolyte which induces spatial proximity of the porphyrin molecules, allowing for their mutual $\pi-\pi$ interaction (brownish solution). This is in analogy to studies on the cooperative binding of dye molecules to linear polyelectrolytes.[69,70]

In this example, the NaPSS brush concentration is 50 mg L^{-1}, which is 240 μM in monomer concentration, and the charge ratio $l = 0.5$. We introduce the charge ratio l being defined as ratio of the molar concentration of positively charged quaternary amine groups of TAPP to the molar concentration of sulfonate groups of the PSS brush

$$l = \frac{c(-\mathrm{NR_3}^+, \mathrm{TAPP})}{c(-\mathrm{SO_3}^-, \mathrm{brush})} \tag{4}$$

At this concentration precipitation of a red aggregate is obtained if the porphyrin is added in charge stochiometry ($l = 1$). Upon increasing the polyelectrolyte concentration, precipitation can be observed even at polyelectrolyte excess, for example with 4.8 mM NaPSS at a charge ratio of $l = 0.5$. Obviously, the porphyrin can act as a linker molecule and interconnect brush molecules to macroscopic objects. The onset of this aggregation depends on both total concentration and charge ratio. In the following we focus on the investigation of samples where no precipitation is observed but aggregates in solution are formed.

The observed color shifts can further be investigated by UV−vis spectroscopy. Figure 3 shows spectra for samples with constant TAPP and CuTAPP concentration and increasing brush concentration. The spectrum of pure TAPP solution as given in Figure 3a,b (upper black line) is in accordance with literature on monomeric TAPP in solutions of low concentrations.[56] Porphyrin spectra usually exhibit two major absorption bands in the visible region: an intense signal between 390 and 425 nm with molar extension coefficients from 2×10^5 to 4×10^5 M^{-1} cm^{-1} usually referred to as Soret or B band resulting from transitions to the second excited singlet state and much weaker Q bands between 500 and 650 nm from transitions to the first excited singlet state, which are split into four signals for free-base porphyrins.[57]

For the brush−porphyrin samples of Figure 3 in contrast to the experiments described in the following sections, the solutions of brush−porphyrin complexes were clear (not turbid) even at excess of porphyrin because of the low concentrations employed. Upon addition of NaPSS brush to excess TAPP solution (Figure 3a), the Soret signal shows hypochromicity of the maximum at 412 nm to 77% at charge stoichiometry ($l = 1$). Additionally, an isosbestic point is present at 423 nm (until $l = 1$). Both indicates that at excess of TAPP there is an equilibrium between free monomeric TAPP molecules and TAPP bound to the polyelectrolyte, likely undergoing mutual $\pi-\pi$ interactions. Interaction with the polystyrene backbone may play an additional role. The conclusion of mutual $\pi-\pi$ interactions is supported by the band splitting into two signals (404 and 418 nm). Both band shape and location of the isosbestic point are similar to results reported for a 20 μM TAPP solution under addition of up to 3.5 M NaCl, leading to self-stacking of porphyrins.[71] Addition of further polyelectrolyte molecules induced a weakening of hypochromicity to 69% at about 10-fold brush excess ($l \approx 0.1$). This may be due to a larger excess of free binding sites of polyelectrolyte that reduce the stacking tendency of porphyrin molecules. It should be noted that the observed band shifts cannot be explained simply by the increase of ionic strength due to NaPSS addition. Adding monomeric *p*-ethylbenzenesulfonate instead of the polyelectrolyte under otherwise identical conditions did not affect band shape and intensity in the concentration regime of TAPP investigated here. A much larger salt concentration would be needed to induce nontemplate mediated self-aggregation of TAPP as was also shown for the addition of sodium chloride.[71]

Furthermore, the spectrum of CuTAPP in Figure 3c, again in agreement with literature for monomeric copper porphyrin spectra (upper black line),[56] exhibits hypochromicity and—in contrast to the metal free TAPP—a strong blue shift upon addition of polyelectrolyte brush. This observation is consistent with the literature on self-aggregation of CuTAPP in aqueous solution induced by salt addition.[56] As can be seen from Figure 3c, the blue-shifted peak increases in intensity at the expense of the monomer signal at 412 nm with an isosbestic point at 403 nm. Therefore, it is reasonable to assign the blue-shifted signal to self-stacking of CuTAPP bound to the NaPSS brush.

The quantitative absorption changes as a function of porphyrin to polyelectrolyte charge ratio (not shown) indicate that binding of the porphyrins to the brush is cooperative; that is, porphyrin molecules preferably bind adjacently to each other. Additionally, the difference in the spectral changes of the two porphyrins upon polyelectrolyte addition should be noted. This difference may be interpreted as the porphyrins having different mutual $\pi-\pi$ stacking geometries on the brush template.[72,73]

B. Imaging of Brush−Porphyrin Aggregates. In the following we focus on imaging structural features that evolve from the association of brush molecules with TAPP. AFM and cryo-TEM images of the NaPSS brush are shown in Figure 4a and Figure 5a. Atomic force microscopy is used to image the structures spin-coated on a mica surface. The brush molecules exhibit a semiflexible cylindrical structure as discussed above. The measured height is 4.0 ± 0.3 nm and is well-defined with only very little variation. This is reasonable because of the high definition in diameter of the cylindrical brushes. Because of interaction with the surface, the brush molecules are flattened on the surface. Cryo-TEM and AFM (Figures 4a and 5a) here are very similar, and thus it can be concluded that the brush structure measured in AFM represents the solution structure. The thickness of NaPSS brushes by cryo-TEM is 10.3 ± 1.3 nm, which is higher than the height on the surface which corresponds to the mentioned flattening effect.

Upon addition of TAPP to the NaPSS brush there is a dramatic change of structural features, as can be seen in Figure 4b. Network-like structures of several 100 nm size are found, in which the previously isolated brush molecules are intercon-

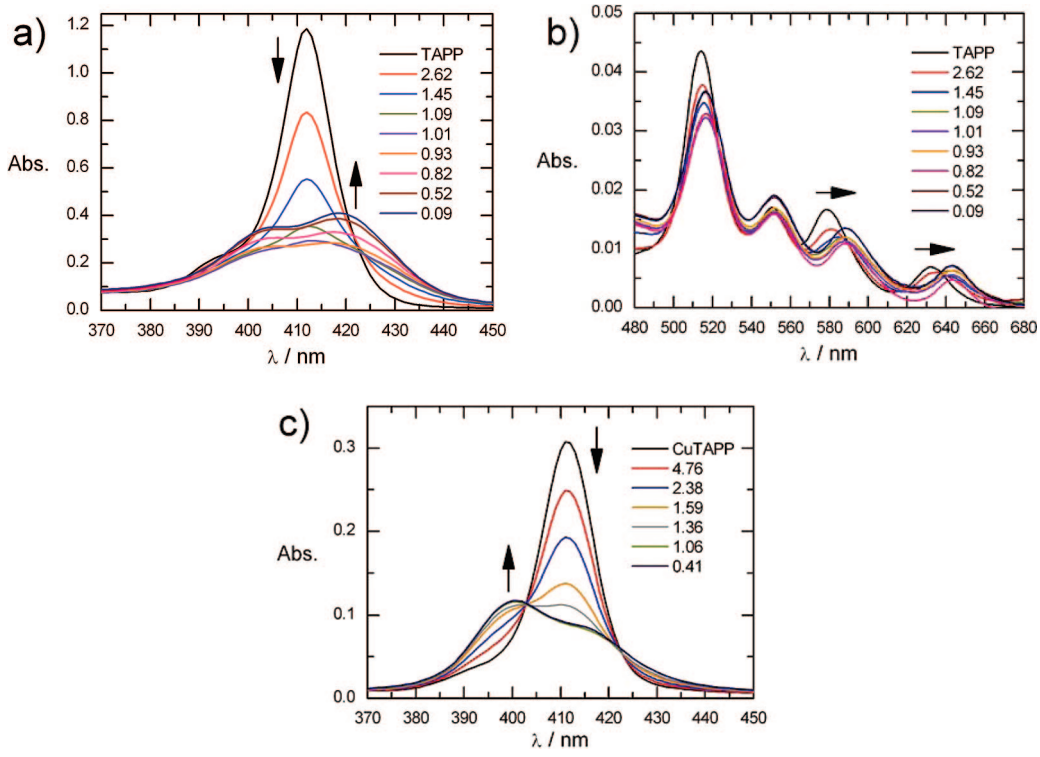

Figure 3. Spectral changes of porphyrin absorption spectra upon addition of polyelectrolyte brush: (a) Soret bands of porphyrin TAPP, $c = 2.85$ μM; (b) Q-bands of (a); (c) porphyrin CuTAPP $c = 0.89$ μM (spectra labeled with porphyrin:NaPSS charge ratio).

nected in an end-to-end fashion. A closer analysis of the network structure at the surface reveals two distinct cylindrical species of different height, as can be easily seen in Figure 4c. The lower species ((1) in Figure 4c) has a measured height of 4.7 ± 0.4 nm, which is close to the height of pure brushes. The second species (2) exhibits a larger height of 7.7 ± 0.5 nm, which is also well-defined. The observed networks mainly consist of the species with larger height. Additionally, in the AFM image there are several sites exhibiting much larger heights (≈ 15 nm, (3)). These are predominantly located at network joints, but there are also network joints without this observation. It should also be noted that the size distribution of the networks is quite broad, from individual brush molecules to networks of 800 nm in diameter.

The formation of these networks thus may be a hierarchical process. The lower height species present in Figure 4b,c most likely represent brush molecules that are not loaded with porphyrin counterions whereas the higher cylindrical parts likely represent brush−porphyrin complexes. This coexistence is consistent with the excess of brush in comparison to porphyrin present in this sample. The even higher parts at the network joints may represent larger porphyrin clusters. The fact that porphyrin-loaded brush and unloaded brush entities are found indicates that porphyrin counterions preferably bind in an accumulated way within the same region, leaving other brushes or brush parts empty rather than distribute uniformly. This would be in accordance with a cooperative binding process as postulated based on the UV−vis results and as known for the binding of dyes to linear polyelectrolytes.[69,70] The observation of network formation is in accordance with experimental and simulation studies described in the literature in that self-assembly of rigid objects often leads to network-like objects, and stiffness likely is a prerequisite for network formation.[55] In addition, comparable experiments of us combining linear flexible PSS with porphyrins yield collapsed structures rather than networks.[74]

As drying and surface interaction effects can modify the structure of objects imaged by AFM, we also used cryo-TEM to investigate the aggregate structures. Results are shown in Figure 5. Comparing the images of aggregates at a surface in AFM and the frozen solution in cryo-TEM shows very similar results. Thus, cryo-TEM confirms the results obtained by AFM, and it can be concluded that brush−porphyrin networks are present in solution. The resolution of Figure 5b was, however, not sufficient to solve the question if the two heights present at the surface also represent the solution structure.

In addition, Figure 6 shows cryo-TEM images obtained from the aggregation of NaPSS brush with copper porphyrin. Here the advantage is a larger contrast provided by the copper. As can be seen from these images, CuTAPP is also capable of interconnecting brush molecules into network-like objects. These networks are structurally very similar to those using TAPP. The higher contrast is again a direct hint that the network structures consist of brush−porphyrin complexes. Additionally, in these images dark areas of higher contrast can be observed that could correspond to clustered porphyrin molecules. This was also observed for aggregates with the metal-free TAPP (Figure 5b). The cryo-TEM images of brush−CuTAPP networks in contrast to the discussed AFM results only exhibit cylindrical molecules of one diameter. However, this could also be due to the much higher contrast of CuTAPP−brush complexes so that brush entities without CuTAPP are not visible. It is of interest to compare the thickness of brush−CuTAPP complexes with the diameter of the pure brush. The measured thickness is 10.1 ± 1.2 nm, which is very close to 10.3 ± 1.3 nm obtained for the pure brush. This is in contrast to the AFM results described above but in accordance with SANS measurements, as will be presented in section D.

Our understanding of the network formation process is the following: first porphyrin molecules associate with the brush template, giving cylindrical brush−porphyrin complexes. These complexes then assemble into a network where tetravalent porphyrin molecules link the complexes. While UV−vis spectroscopy indicates a difference in the stacking geometry of TAPP and CuTAPP, the general observation of network formation is the same for both. Thus, AFM and cryo-TEM reveal the formation of a new type of nanoscale structure: finite-size

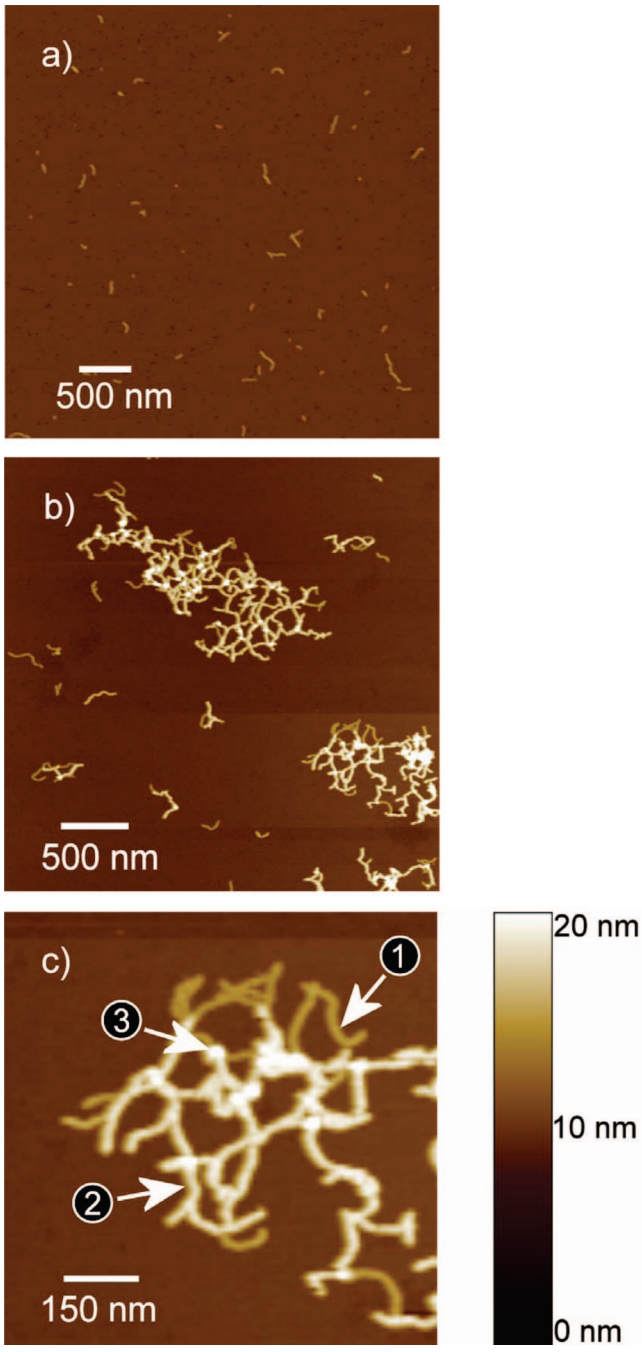

Figure 4. AFM images of brush and brush−porphyrin aggregates spin-coated on a mica surface: (a) pure brush; (b) brush + TAPP, charge ratio $l = 0.5$; (c) enlarged view of (b) (all: c(NaPSS) = 240 μM).

networks from cylindrical polyelectrolyte brushes with porphyrin counterions that are stable in aqueous solution and can be obtained with free porphyrin as well as with metal ion-containing porphyrins.

C. Light Scattering of Brush−Porphyrin Aggregates. While AFM and cryo-TEM clearly image the structural type of the aggregates, they also reveal that their size distribution is quite broad and do not allow for a quantitative analysis of the average network size. For this purpose the solutions were analyzed by light scattering.

Dynamic light scattering of the (pure) PSS brush yielded in all cases only one diffusion process, and the dependence on added salt concentration was small. Thus, no complication by polyelectrolyte effects[61,75−81] is expected, and diffusion coefficients can be treated as self-diffusion coefficients and translated into hydrodynamic radii.

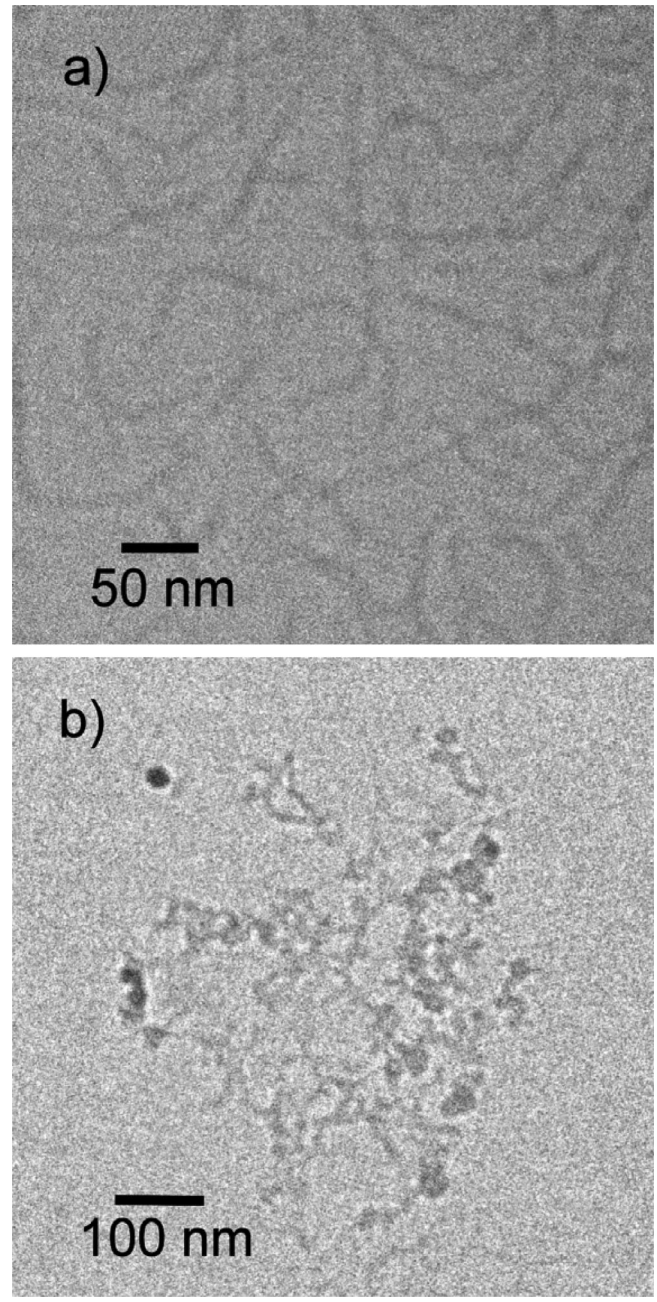

Figure 5. Cryo-TEM images of brush and brush−porphyrin aggregates: (a) pure brush; (b) brush + TAPP, charge ratio $l = 0.5$ (all: c(NaPSS) = 2.4 mM).

The characterization of the TAPP−brush complexes by routine light scattering is accompanied by complications as TAPP absorbs light of the wavelength general used in laser light scattering in the red or green region. Therefore, we have built a light scattering setup (Figure 7) combining an infrared laser diode (λ = 831.5 nm) for measuring samples containing porphyrins and a conventional He−Ne laser (λ = 632.8 nm) for nonabsorbing solutions. At the wavelength of the IR laser there is no light absorption by the porphyrin (see Figure 3b). By dynamic light scattering on the NaPSS brush (without porphyrin) and polystyrene standards, we showed that both lasers gave the same data for angular dependent measurements and resulting hydrodynamic radii. Thus, we concluded that the IR laser gives consistent results for hydrodynamic radii of the samples analyzed in this study.

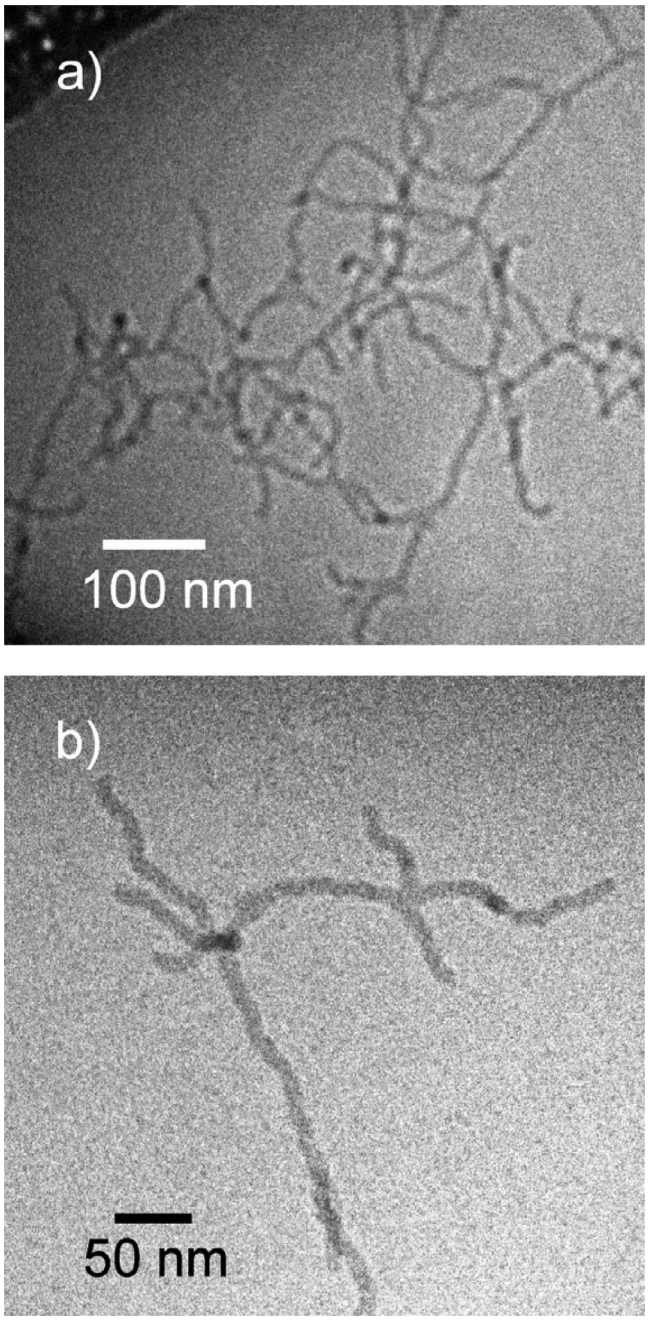

Figure 6. Cryo-TEM images of brush−CuTAPP aggregates; charge ratio $l = 0.5$, c(NaPSS) = 2.4 mM.

As the imaging techniques revealed large sizes of the aggregated structures (up to several 100 nm), we filtered the solutions of the components separately prior to the LS experiment in order to avoid sample loss or structural changes upon filtering. By UV−vis absorption spectroscopy, we confirmed that no filtration loss of these stock solutions occurred. As will be described in section E, we have carefully analyzed the influence of sample preparation on the size of brush polyelectrolyte networks measured by dynamic light scattering. It was found that the procedure of adding a stock solution of porphyrin TAPP to a brush solution upon stirring gives well-reproducible hydrodynamic radii and was thus used for the samples described in the following. Brush−porphyrin aggregates are prepared in salt-free aqueous solution. Addition of salt for analytic purposes (to avoid polyelectrolyte effects) is not the choice here as it may change the aggregation behavior (see section F). Therefore, we have chosen a low polymer concentration instead (which is

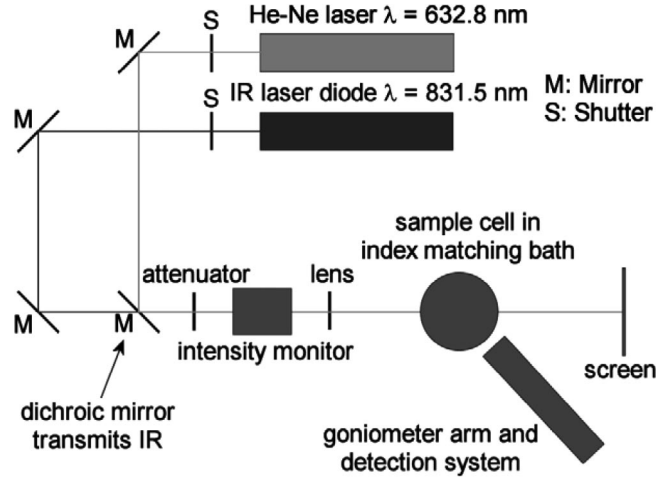

Figure 7. Light scattering setup combining an infrared laser diode and a He−Ne laser.

possible due to the strong scattering power of the brush and its complexes). As at this concentration the polymer brush shows only one diffusion mode, not much interaction effects are to be expected for the networks where even more charges may be neutralized by condensed porphyrin counterions. In addition, a small amount of salt (sodium tosylate) is inherently present from the initial counterions of brush and TAPP.

We have shown above that at a polyelectrolyte concentration of 240 μM brush−porphyrin aggregates of finite size were obtained at polyelectrolyte excess. It is of interest to investigate the size of networks in solution and which parameters control that size. As was concluded based on the onset of precipitation (see section A), the absolute concentration and the ratio of porphyrin to polyelectrolyte play a key role. In the following we will focus on the influence of the ratio of porphyrin to polyelectrolyte on the networks formed in solution. Given a constant brush concentration, the addition of further porphyrin linker molecules is expected to increase the network size. Figure 8 displays the size change from brush to network according to the samples described in section B as determined by dynamic light scattering. The time autocorrelation function is shifted to higher relaxation times due to aggregation of brush molecules. We have used a second-order cumulant method to evaluate the angle-dependent diffusion coefficient (Figure 8a) and extrapolated these to zero scattering vector square (not shown). Employing this analysis in the transition region from individual brush molecules to macroscopic precipitation, a range of stable aggregates in solution was detected for $0 < l < 0.7$. Above $l = 0.7$ precipitation takes place when mixing the component solutions. Figure 8b shows the hydrodynamic radius as a function of charge ratio. In the range $0 < l < 0.6$, the average network size shows a linear dependence on porphyrin concentration with increasing hydrodynamic radius from the brush size to about $R_H = 80$ nm. Above $l = 0.6$ the radius starts to diverge with a maximum size for stable aggregates in solution of $R_H = 130$ nm at $l = 0.7$. In particular, for the smaller network radii at low l it must be noted that R_H represents an average value (inverse z-average) and may result from a mixture of individual brushes and networks.

Additionally, we have used cumulant analysis to estimate the size distribution of networks. We use a polydispersity index (PDI) defined as PDI $= \mu_2/(\Gamma)^2$, Γ and μ_2 (eq 1) being the first and second cumulant, respectively. We have shown that the PDI at scattering angle $\theta = 90°$ increases from 0.18 for the pure brush to 0.27 upon complexation with TAPP at charge ratio 0.5. As the network size distribution is quite broad, it is surprising that a clear linear dependence of the average radius

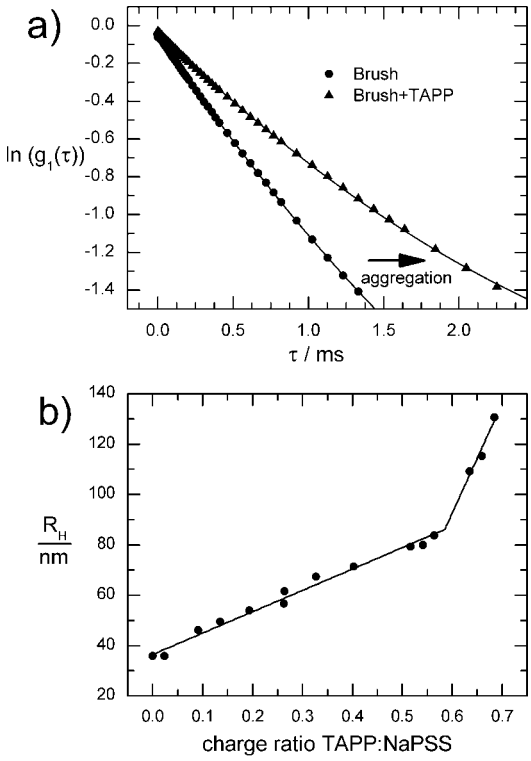

Figure 8. Dynamic light scattering on brush−TAPP samples in aqueous solution ($\lambda = 831.5$ nm): (a) second-order cumulant evaluation of the electric field autocorrelation function at scattering angle $\theta = 90°$ for NaPSS brush ($c = 240$ μM) and brush + porphyrin (c(NaPSS) = 240 μM, charge ratio $l = 0.4$); (b) hydrodynamic radius (inverse z-average) as a function of charge ratio TAPP:NaPSS (= l as given in eq 4), c(NaPSS) = 50 mg L^{-1} (240 μM).

on charge ratio is observed. These sizes are well-reproducible, and the finite-size networks are stable in solution with constant hydrodynamic radii for several months. This also indicates that the varying ionic strength due to the increasing amount of tosylate ions with increasing TAPP concentration is not expected to have a tremendous influence on the results, which is reasonable as it is low (3×10^{-5} M at $l = 0.5$; only at much higher salt concentrations such as 0.01 M a time-dependent decrease of network size was observed, but even then not on the time scale of these measurements; see section F). Thus, the charge ratio of porphyrin to polyelectrolyte is a parameter which can be used to adjust the average size of mesoscale assembled networks in aqueous solution.

For comparison, we have in addition combined porphyrin with monomeric *p*-ethylbenzenesulfonate (NaSS). At c(NaSS) = 240 μM and c(TAPP) = 30 μM, charge ratio $l = 0.5$, there is no time correlation function measurable, and the scattering intensity is comparable to water. Thus, one can conclude that TAPP does not self-aggregate at $c = 30$ μM, and its aggregation on brush molecules is due to the polyelectrolyte nature of the template.

D. Small-Angle Neutron Scattering of Brush−Porphyrin Aggregates. To analyze the structure of brush−porphyrin aggregates in solution on a smaller size scale, small-angle neutron scattering (SANS) was performed. Results are shown in Figure 9. Figure 9a shows scattering curves for the NaPSS brush in D_2O, 0.01 M NaCl, and a brush−porphyrin aggregate in D_2O. All scattering curves show the shape typical of wormlike chains.[41,42] This is to be expected as the overall network size is not covered in this experiment where the q range approximately covers a size range of up to 185 nm. The scaling in the linear part is -1.40 ± 0.05. SANS is of particular interest to resolve the cross-sectional dimension. Cross-section Guinier plots are

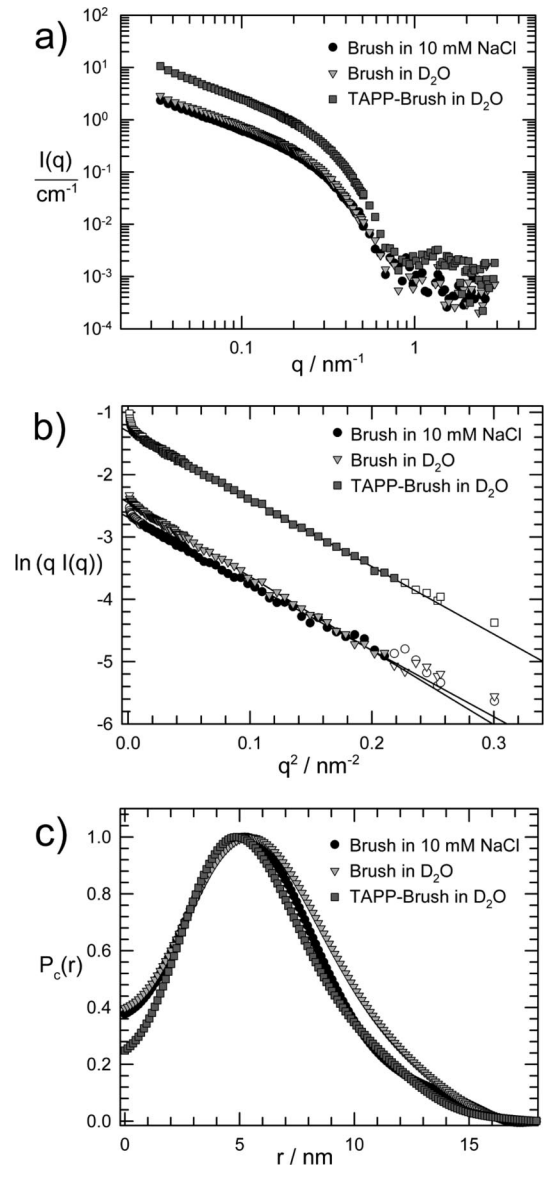

Figure 9. Small-angle neutron scattering of cylindrical NaPSS brush in 10 mM NaCl solution, in salt-free solution, and TAPP−brush complex ($l = 0.5$) in salt-free solution: (a) scattering curves $I(q)$, (b) cross-section Guinier plot (filled symbols were included in the Guinier extrapolation), (c) normalized cross-sectional pair distance distribution functions $P_c(r)$, c(NaPSS) = 1 g L^{-1} (4.8 mM).

shown in Figure 9b. The linear dependence proves the rodlike structure. Quantitatively, resulting cross-sectional radii of gyration $R_{G,c}$ are $R_{G,c} = 4.9 \pm 0.1$ nm for the brush in salt-free solution, $R_{G,c} = 4.6 \pm 0.1$ nm for the brush in NaCl solution, and $R_{G,c} = 4.6 \pm 0.1$ nm for the brush−porphyrin network. Thus, the brush in salt solution shows a slightly smaller $R_{G,c}$ than in salt-free aqueous solution while the porphyrin−brush complex again shows the same $R_{G,c}$ as the brush in salt solution. In front of the AFM results, this may be a surprising result. Obviously, in solution the porphyrin counterions associate with the polyelectrolyte brush in such a way that its cross-sectional radius of gyration is not changed. Thus, the two different heights of the brush and brush−porphyrin parts are only caused by surface interactions when preparing the AFM samples. This is in accordance with the cryo-TEM observation that brush−CuTAPP complexes show the same diameter as pure brushes (section B).

Figure 9c shows cross-sectional pair distance distribution functions $P_c(r)$ that are obtained from the scattering curve by

indirect Fourier transformation.[64−67] The $P_c(r)$ gives the number of distances within the diameter as a function of distance and is thus typical of the radial density profile. It allows to analyze the form factor oscillations at high q while only "assuming" cylindrical geometry (as deduced from the cross-section Guinier plots) but not a priori any specific "arbitrarily chosen" model for the type of density profile. Again, it can be seen that all three samples are quite similar. The total diameter is between 17 and 18 nm. The $R_{G,c}$ values corresponding to these $P_c(r)$ functions are in good agreement with the ones from Guinier analysis. The slight decrease in brush diameter upon salt addition is again visible, while the complex more resembles the brush in salt solution rather than in salt-free solution. This may be understood by the fact that binding of porphyrin decreases the brush net charge. The density distribution is very similar to the brush in NaCl. However, as compared to the brush in NaCl, the maximum is slightly shifted to the inside, and $P_c(r)$ is less expressed at larger r, indicating a slight shift of the main density contribution toward the interior.[82]

It is important to note that if two different species are present as we concluded from AFM results, pure brush and brush−porphyrin cylindrical parts, the $P_c(r)$ represents an overlay of the two $P_c(r)$ functions. However, a clearly altered density profile or thickness change in 50% of the cylindrical species would be clearly visible also in the averaged $P_c(r)$. Thus, SANS clearly shows that no significant thickness change of the brush upon binding of porphyrin is observed in solution.

While the normalized scattering curves of brush and complex almost exactly overlay (not shown) and thus structural parameters including persistence length are very similar, there is a clear difference in absolute scattering intensity (Figure 9a). The difference in scattering intensity on an absolute scale (differential scattering cross section in cm^{-1}) can be translated into an estimate for the number of porphyrin molecules per brush unit, assuming in a first approximation that the partial specific volume at infinite dilution is constant, which represents a common approach for diluted polymer solutions.[63] The result is consistent with the added porphyrin at $l = 0.5$ being completely bound to the brush. The amount can be determined more exactly by analytical ultracentrifugation, which showed that no excess porphyrin stays in solution when the complex sediments, that is, the porphyrin is completely (>98%) bound to the brush.

E. Influence of Sample Preparation. When investigating self-assembly processes, it is of interest whether the resulting structures depend on the preparation procedure, i.e., are kinetically frozen, or represent equilibrium structures, which usually means the same structures can be obtained via different preparation routes. While complexes of two oppositely charged polyelectrolytes usually represent kinetically trapped structures due to the high number of charges,[18,19] recently described assemblies of ionic dendrimers with divalent dye counterions were shown to be equilibrium structures.[27−29] On the basis of charge numbers, the system investigated here may be considered as "in between", and thus the influence of sample preparation is highly interesting.

The samples presented above were prepared by the procedure of adding porphyrin to brush, since in this case it is assured that during sample preparation there is always excess of brush. This may be important since complexes may precipitate in excess of porphyrin. So if during preparation the regime of the "phase diagram" were the sample usually precipitates is crossed, it may be that the precipitate formed is not redissolved because of kinetic trapping. A clear solution as final thermodynamic state may not be reached.

Adding porphyrin to brush to reach a final brush concentration of c(NaPSS) = 240 μM and charge ratio $l = 0.5$ gives a clear solution. Dynamic light scattering yielded different results depending on the exact way of preparation: lower radii (R_H = 71−76 nm) which are well reproducible if the samples were stirred during dropwise addition of porphyrin and higher radii (R_H = 147−183 nm) with lower definition in size if TAPP was added to a still solution and the sample mixed after the addition of each drop (Table 1). The origin of this observation may lie in the temporary distribution of TAPP molecules throughout the sample. When one drop of porphyrin is added to a still brush solution locally, a small volume with higher TAPP concentration and thus excess of TAPP relative to brush molecules is created. Some very large aggregates may form locally that do not redissolve later, and thus a larger ensemble averaged hydrodynamic radius results. Hence, structures resulting from the preparation without stirring may be considered kinetically controlled. In contrast, if the porphyrin is added to a turbulent brush solution, TAPP will be immediately distributed throughout the total sample volume and local porphyrin excess can be avoided. Therefore, we focused on the preparation via addition of porphyrin to brush under stirring and all samples discussed in section E were prepared via this route. Both resulting network sizes stayed constant for several months.

Table 1. Results for TAPP−Brush Samples Obtained by Different Preparation Methods, c(NaPSS) = 240 μM, $l = 0.5$

	TAPP to brush	brush to TAPP
no stirring	final solution: clear R_H = 147−183 nm	final solution: clear R_H = 193−290 nm intermediate turbidity at $l = 2.8$
stirring	final solution: clear R_H = 71−76 nm	final solution: turbid intermediate turbidity at $l = 2.8$

To further investigate the influence of sample preparation on network size, we have also applied the opposite procedure, that is, adding the brush solution to a porphyrin solution. Upon addition of the third drop of brush solution ($l = 2.8$) turbidity was observed (for both stirring and not). Distinguishing "clear" and "turbid" thereby is most obvious by looking at a screen showing the transmitted laser beam pattern. Addition of further drops to reach c(NaPSS) = 240 μM and $l = 0.5$ under stirring caused the sample to remain turbid. In contrast, without stirring the solution went back to clear. The explanation may again be related to the distribution of components—here the NaPSS brush—during addition.

Thus, in combination it may be concluded that, in particular under stirring, results strongly depend on the sequence of component addition. However, this does not necessarily mean that by the preparation method chosen in the main part of this study (addition of porphyrin to brush under stirring) the aggregates were kinetically trapped. The reason for the influence of preparation technique may rather be within the phase regimes that are crossed during sample preparation in case of intermediate precipitation (or intermediate formation of larger aggregates) in porphyrin excess. Therefore, as mentioned above, our chosen preparation method avoids crossing this regime. Results of this section show the importance of investigating variations in the preparation procedure for the self-assembly of strongly interacting building blocks.

F. Brush−Porphyrin Aggregates in Salt Solution. As the structures formed are based on ionic interaction, addition of low-molecular-mass salt such as NaCl should influence the structure formation due to screening of electrostatics. Therefore, NaCl solution was added to a stable brush−TAPP sample with l = 0.5 that was previously prepared in salt-free solution. Time-dependent light scattering experiments show a decrease of the hydrodynamic radius from R_H = 77 nm to R_H = 32 nm within 1−2 days when the salt-free sample was prepared by stirring and from R_H = 183 nm to R_H = 28 nm within 8 h when there was no stirring during sample preparation. The final hydrodynamic radius represents the size of the NaPSS brush only; that

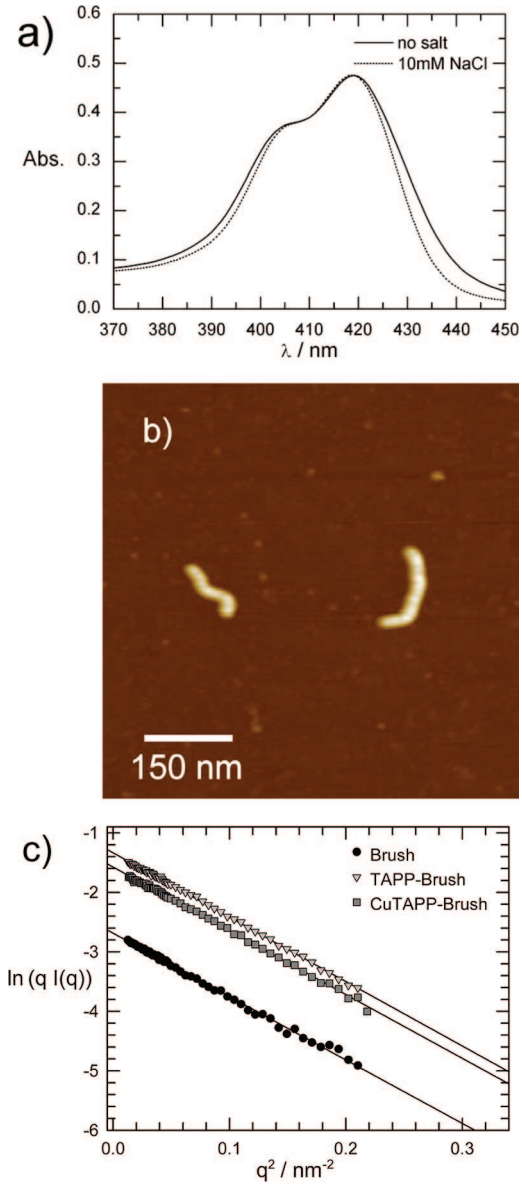

Figure 10. Behavior of brush−porphyrin complexes upon salt addition (c(NaPSS) = 240 μM, l = 0.5, c(NaCl) = 10 mM): (a) UV−vis spectra; (b) AFM height image (height scale as in Figure 4; (c) small-angle neutron scattering of NaPSS brush in 10 mM NaCl solution, TAPP−brush complex (l = 0.5) in 10 mM NaCl and CuTAPP−brush complex (l = 0.5) in 10 mM NaCl: cross-section Guinier plot (filled symbols were included in the Guinier extrapolation).

is, networks are disconnected upon salt addition and individual brush molecules remain. Figure 10a shows UV−vis spectra of the resulting brush samples. The spectrum is the one typical of the porphyrin−NaPSS complexes with stacked porphyrins in difference to the spectrum of the noninteracting porphyrins. Thus, the network is dissolved but the porphyrin molecules stay connected with the brush. This is confirmed by the AFM image Figure 10b which shows individual brushes with larger height (7.7 ± 0.7 nm) than the pure brush, in accordance with brush−porphyrin complexes present in the networks.

Because of the added salt, the AFM sample preparation was different from the one in Figure 4. Freshly cleaved mica was exposed to the sample solution for 5 min and extensively rinsed with water afterward. The possibility to immobilize the brush−porphyrin complexes on the negatively charged mica surface indicates that the brush−porphyrin complex is positively charged; that is, there is charge inversion of the polyelectrolyte upon complexation of NaPSS with TAPP. For comparison, negatively charged (pure) NaPSS brushes cannot be immobilized on a mica surface by the same method.

Figure 10c shows SANS results of samples in salt solution as cross-section Guinier representation. Again scattering curves (not shown) differ in intensity but almost not in shape. Thus, no substantial change of brush thickness, density profile, and persistence length of the brush−porphyrin complex as compared to the brush is observed in solution. Cross-section Guinier plots reveal a radius of gyration $R_{G,c}$ = 4.6 ± 0.1 nm that does not differ whether TAPP or CuTAPP is used, even though the band shifts in UV−vis spectroscopy (section A) indicate a different stacking behavior of TAPP and CuTAPP on the brush template. Likewise, the cross-section pair distance distribution $P_c(r)$ function (not shown) again indicates almost no change in the cross-sectional dimensions. The fact that the structural features stay unchanged upon porphyrin binding is of particular interest because brush−surfactant complexes in organic solvent in contrast show an increase in diameter and a decrease in persistence length.[42]

These results again demonstrate the hierarchical structure formation of networks investigated in this study, where the higher-level networks are dissolved upon salt addition. This finding proves that this level is based on electrostatic interactions. The first level of organization remains intact even in a salt solution of 10 mM NaCl. This is reasonable as electrostatics is strong here with tetravalent TAPP counterions as opposed to monovalent screening ions and particularly since additional $\pi-\pi$ interactions are possible. Thus, by addition of salt single PSS brushes decorated with porphyrins can be obtained. These may be interesting as functional molecular assemblies. Porphyrin stacks are of interest for many reasons, molecular electronics, and photoconductivity being only examples. The polymer template here may provide a much more stable and size-controlled assembly than porphyrin stacks investigated by other authors. Thus, this structure could provide an important model system, but also mechanical stability and processability may make it more appropriate for applications. On the other hand, the brush−porphyrin networks may combine special optical and mechanical properties. In addition, the possibility to disconnect the network by facile salt addition may also be interesting for potential applications that rely on the network properties responding to added salt or otherwise caused changes in the environmental ionic strength. These issues will be topics of future studies.

Conclusions

We have investigated electrostatic self-assembly of cylindrical polyelectrolyte brushes with organic counterions of different valency. While monovalent and divalent counterions cause no expressed structural changes, tetravalent cationic porphyrins can connect the brushes into finite-size networks in solution. The porphyrins bind to the polyelectrolyte brushes due to electrostatics and secondary mutual $\pi-\pi$ interactions on a first hierarchical level and due to their tetravalent nature cause aggregation of multiple brushes on a higher order. Structures have been characterized by UV−vis spectroscopy, AFM, cryo-TEM, SANS, and DLS, and different preparation methods were compared. In sodium chloride solution individual brushes decorated with porphyrins are formed. Thus, two new supramolecular structures, finite-size networks, and porphyrin-decorated cylindrical brushes were obtained. Both are stable in aqueous solution and can be deposited on surfaces as intact structure. The new morphologies have potential as functional materials with unique mechanical and optical properties, in molecular electronics or in pharmaceutics.

Acknowledgment. We thank Dr. R. Berger and U. Rietzler for help with AFM measurements, Dr. S. Duschner for her contribution

to the NaPSS brush synthesis, Dr. H. Frielinghaus (JCNS, FRMII) and Drs. R. Schweins and P. Lindner (ILL) for support with SANS experiments, Dr. H. Cölfen for AUZ, Prof. Dr. W. Steffen for support with infrared light scattering, and K. Klein for her contributions to this work. We are thankful to Prof. Dr. G. Wegner and Prof. Dr. M. Schmidt for fruitful discussions. Financial support of the Max Planck Society, Deutsche Forschungsgemeinschaft (SFB 625), ILL, and the POLYMAT Graduate School of Excellence (University of Mainz) is gratefully acknowledged.

References and Notes

(1) Lehn, J. M. *Supramolecular Chemistry: Concepts and Perspectives*; Wiley-VCH: Weinheim, 1995.
(2) Ringsdorf, H.; Schlarb, B.; Venzmer, J. *Angew. Chem., Int. Ed.* **1988**, *27*, 113–158.
(3) Zhang, L. F.; Eisenberg, A. *Science* **1995**, *268*, 1728–1731.
(4) Discher, D. E.; Eisenberg, A. *Science* **2002**, *297*, 967–973.
(5) Antonietti, M.; Förster, S. *Adv. Mater.* **2003**, *15*, 1323–1333.
(6) Pochan, D. J.; Chen, Z. Y.; Cui, H. G.; Hales, K.; Qi, K.; Wooley, K. L. *Science* **2004**, *306*, 94–97.
(7) Sijbesma, R. P.; Beijer, F. H.; Brunsveld, L.; Folmer, B. J. B.; Hirschberg, J. H. K. K.; Lange, R. F. M.; Lowe, J. K. L.; Meijer, E. W. *Science* **1997**, *278*, 1601–1604.
(8) Schmuck, C.; Wienand, W. *Angew. Chem., Int. Ed.* **2001**, *40*, 4363–4369.
(9) Schlaad, H.; Krasia, T.; Antonietti, M. *J. Am. Chem. Soc.* **2004**, *126*, 11307–11310.
(10) Kaiser, T. E.; Wang, H.; Stepanenko, V.; Würthner, F. *Angew. Chem., Int. Ed.* **2007**, *46*, 5541–5544.
(11) Lehn, J. M. *Angew. Chem., Int. Ed.* **1988**, *27*, 89–112.
(12) Antonietti, M.; Conrad, J.; Thünemann, A. *Macromolecules* **1994**, *27*, 6007–6011.
(13) Rädler, J. O.; Koltover, I.; Salditt, T.; Safinya, C. R. *Science* **1997**, *275*, 810–814.
(14) Koltover, I.; Salditt, T.; Rädler, J. O.; Safinya, C. R. *Science* **1998**, *281*, 78–81.
(15) Thünemann, A. F.; Beyermann, J. *Macromolecules* **2000**, *33*, 6878–6885.
(16) Faul, C. F. J.; Antonietti, M. *Adv. Mater.* **2003**, *15*, 673–683.
(17) Zakrevskyy, Y.; Stumpe, J.; Faul, C. F. J. *Adv. Mater.* **2006**, *18*, 2133.
(18) Thünemann, A. F.; Müller, M.; Dautzenberg, H.; Joanny, J. F. O.; Löwen, H. *Adv. Polym. Sci.* **2004**, *166*, 113–171.
(19) Störkle, D.; Duschner, S.; Heimann, N.; Maskos, M.; Schmidt, M. *Macromolecules* **2007**, *40*, 7998–8006.
(20) Ikeda, Y.; Beer, M.; Schmidt, M.; Huber, K. *Macromolecules* **1998**, *31*, 728–733.
(21) Peng, S. F.; Wu, C. *Macromolecules* **1999**, *32*, 585–589.
(22) Schweins, R.; Huber, K. *Eur. Phys. J. E* **2001**, *5*, 117–126.
(23) Lin, W.; Zhou, Y. S.; Zhao, Y.; Zhu, Q. S.; Wu, C. *Macromolecules* **2002**, *35*, 7407–7413.
(24) Schweins, R.; Lindner, P.; Huber, K. *Macromolecules* **2003**, *36*, 9564–9573.
(25) Schweins, R.; Goerigk, G.; Huber, K. *Eur. Phys. J. E* **2006**, *21*, 99–110.
(26) Goerigk, G.; Huber, K.; Schweins, R. *J. Chem. Phys.* **2007**, *127*, 154908.
(27) Gröhn, F.; Klein, K.; Brand, S. *Chem.—Eur. J.* **2008**, *14*, 6866–6869.
(28) Gröhn, F. *Macromol. Chem. Phys.* **2008**, *209*, 2295–2301.
(29) Willerich, I.; Gröhn, F. *Chem.—Eur. J.* **2008**, *14*, 9083−9116.
(30) Wintermantel, M.; Schmidt, M.; Tsukahara, Y.; Kajiwara, K.; Kohjiya, S. *Macromol. Rapid Commun.* **1994**, *15*, 279–284.
(31) Wintermantel, M.; Gerle, M.; Fischer, K.; Schmidt, M.; Wataoka, I.; Urakawa, H.; Kajiwara, K.; Tsukahara, Y. *Macromolecules* **1996**, *29*, 978–983.
(32) Dziezok, P.; Sheiko, S. S.; Fischer, K.; Schmidt, M.; Möller, M. *Angew. Chem., Int. Ed.* **1997**, *36*, 2812–2815.
(33) Gerle, M.; Fischer, K.; Roos, S.; Müller, A. H. E.; Schmidt, M.; Sheiko, S. S.; Prokhorova, S.; Möller, M. *Macromolecules* **1999**, *32*, 2629–2637.
(34) Schlüter, A. D.; Rabe, J. P. *Angew. Chem., Int. Ed.* **2000**, *39*, 864–883.
(35) Cheng, G. L.; Boker, A.; Zhang, M. F.; Krausch, G.; Müller, A. H. E. *Macromolecules* **2001**, *34*, 6883–6888.
(36) Pyun, J.; Kowalewski, T.; Matyjaszewski, K. *Macromol. Rapid Commun.* **2003**, *24*, 1043–1059.
(37) Rühe, J.; Ballauff, M.; Biesalski, M.; Dziezok, P.; Gröhn, F.; Johannsmann, D.; Houbenov, N.; Hugenberg, N.; Konradi, R.; Minko, S.; Motornov, M.; Netz, R. R.; Schmidt, M.; Seidel, C.; Stamm, M.; Stephan, T.; Usov, D.; Zhang, H. N. *Adv. Polym. Sci.* **2004**, *165*, 79–150.
(38) Lienkamp, K.; Ruthard, C.; Lieser, G.; Berger, R.; Gröhn, F.; Wegner, G. *Macromol. Chem. Phys.* **2006**, *207*, 2050–2065.
(39) Lienkamp, K.; Noe, L.; Breniaux, M. H.; Lieberwirth, I.; Gröhn, F.; Wegner, G. *Macromolecules* **2007**, *40*, 2486–2502.
(40) Sheiko, S. S.; Sumerlin, B. S.; Matyjaszewski, K. *Prog. Polym. Sci.* **2008**, *33*, 759–785.
(41) Zhang, B.; Gröhn, F.; Pedersen, J. S.; Fischer, K.; Schmidt, M. *Macromolecules* **2006**, *39*, 8440–8450.
(42) Duschner, S.; Gröhn, F.; Maskos, M. *Polymer* **2006**, *47*, 7391–7396.
(43) Wasielewski, M. R. *Chem. Rev.* **1992**, *92*, 435–461.
(44) Lin, V. S. Y.; Dimagno, S. G.; Therien, M. J. *Science* **1994**, *264*, 1105–1111.
(45) Gust, D.; Moore, T. A.; Moore, A. L. *Acc. Chem. Res.* **2001**, *34*, 40–48.
(46) Guldi, D. M. *Chem. Soc. Rev.* **2002**, *31*, 22–36.
(47) Schwab, A. D.; Smith, D. E.; Bond-Watts, B.; Johnston, D. E.; Hone, J.; Johnson, A. T.; de Paula, J. C.; Smith, W. F. *Nano Lett.* **2004**, *4*, 1261–1265.
(48) Meunier, B. *Chem. Rev.* **1992**, *92*, 1411–1456.
(49) Bonnett, R. *Chem. Soc. Rev.* **1995**, *24*, 19–33.
(50) Dougherty, T. J.; Gomer, C. J.; Henderson, B. W.; Jori, G.; Kessel, D.; Korbelik, M.; Moan, J.; Peng, Q. *J. Natl. Cancer Inst.* **1998**, *90*, 889–905.
(51) Sternberg, E. D.; Dolphin, D.; Brückner, C. *Tetrahedron* **1998**, *54*, 4151–4202.
(52) Terech, P.; Weiss, R. G. *Chem. Rev.* **1997**, *97*, 3133–3159.
(53) Lee, K. Y.; Mooney, D. J. *Chem. Rev.* **2001**, *101*, 1869–1879.
(54) Oh, J. K.; Drumright, R.; Siegwart, D. J.; Matyjaszewski, K. *Prog. Polym. Sci.* **2008**, *33*, 448–477.
(55) Sayar, M.; Stupp, S. I. *Phys. Rev. E* **2005**, *72*, 011803.
(56) Bütje, K.; Nakamoto, K. *Inorg. Chim. Acta* **1990**, *167*, 97–108.
(57) Gouterman, M. In *The Porpyrins - Physical Chemistry, Part A*; Dolphin, D., Ed.; Academic Press: New York, 1978; Vol. *3*, pp 1−165.
(58) Tsukahara, Y.; Mizuno, K.; Segawa, A.; Yamashita, Y. *Macromolecules* **1989**, *22*, 1546–1552.
(59) Tsukahara, Y.; Tsutsumi, K.; Yamashita, Y.; Shimada, S. *Macromolecules* **1990**, *23*, 5201–5208.
(60) Hugenberg, N.; Loske, S.; Müller, A. H. E.; Schärtl, W.; Schmidt, M.; Simon, P. F. W.; Strack, A.; Wolf, B. A. *J. Non-Cryst. Solids* **2002**, *307*, 765–771.
(61) Gröhn, F.; Antonietti, M. *Macromolecules* **2000**, *33*, 5938–5949.
(62) Duschner, S. PhD Thesis, University of Mainz, **2007**.
(63) Lindner, P., Zemb, T., Eds.; *Neutrons, X-rays, and Light: Scattering Methods Applied to Soft Condensed Matter*; Elsevier: Amsterdam, 2002.
(64) Glatter, O. *Acta Phys. Austriaca* **1977**, *47*, 83–102.
(65) Glatter, O. *J. Appl. Crystallogr.* **1977**, *10*, 415–421.
(66) Glatter, O. *J. Appl. Crystallogr.* **1980**, *13*, 577–584.
(67) Gröhn, F.; Bauer, B. J.; Amis, E. J. *Macromolecules* **2001**, *34*, 6701–6707.
(68) Ashley, J. N.; Leeds, W. G. *J. Chem. Soc.* **1957**, 2706−2713.
(69) Schwarz, G.; Klose, S.; Balthasar, W. *Eur. J. Biochem.* **1970**, *12*, 454–460.
(70) Horn, D. *Prog. Colloid Polym. Sci.* **1978**, *65*, 251–264.
(71) Kano, K.; Takei, M.; Hashimoto, S. *J. Phys. Chem.* **1990**, *94*, 2181–2187.
(72) Kasha, M.; Rawls, H. R.; El-Bayoumi, M. A. *Pure Appl. Chem.* **1965**, *11*, 371–392.
(73) Kasha, M.; El-Bayoumi, M. A.; Rhodes, W. *J. Chim. Phys. Phys.-Chim. Biol.* **1961**, *58*, 916–925.
(74) Ruthard, C.; Gröhn, F., recent results.
(75) Förster, S.; Schmidt, M.; Antonietti, M. *Polymer* **1990**, *31*, 781–792.
(76) Sedlak, M.; Amis, E. J. *J. Chem. Phys.* **1992**, *96*, 826–834.
(77) Schmitz, K. S. *Macroions in Solution and Colloidal Suspension*; Wiley-VCH: New York, 1993.
(78) Gröhn, F.; Topp, A.; Belkoura, L.; Woermann, D. *Ber. Bunsen-Ges. Phys. Chem.* **1995**, *99*, 736–740.
(79) Ermi, B. D.; Amis, E. J. *Macromolecules* **1998**, *31*, 7378–7384.
(80) Antonietti, M.; Briel, A.; Gröhn, F. *Macromolecules* **2000**, *33*, 5950–5953.
(81) Antonietti, M.; Briel, A.; Gröhn, F. In *Structure and Dynamics of Polymer and Colloidal Systems;* Borsali, R., Pecora, R., Eds.; Kluwer: Dordrecht, 2002; p 363.
(82) The fact that $P_c(r)$ does not decrease to 0 at $P(0)$ is due to resolution problems (determined by q_{max}). The difference in this region thus has no physical meaning. The finite intercept is also the reason why deconvolution into a density profile is not possible; compare also ref 67.

MA802038Q